

Probing the octant of θ_{23} with very long baseline neutrino oscillation experiments: a global look

Guey-Lin Lin^{a,b*} and Yoshiaki Umeda^{a†}

^a*Institute of Physics, National Chiao-Tung University, Hsinchu 300, Taiwan*

^b*Physics Division, National Center for Theoretical Sciences, Hsinchu 300, Taiwan*

(Dated: June 24, 2018)

Abstract

We investigate the baseline range in which the θ_{23} degeneracy in neutrino oscillation probabilities is absent for fixed values of θ_{13} and CP violation phase δ_{CP} . We begin by studying sensitivities of neutrino oscillation probabilities to θ_{13} , θ_{23} and δ_{CP} for very-long-baseline neutrino oscillations. We show contour graphs of the muon-neutrino survival probability $P(\nu_\mu \rightarrow \nu_\mu)$ and the appearance probability $P(\nu_e \rightarrow \nu_\mu)$ on the $\cos 2\theta_{23} - \sin 2\theta_{13}$ plane for baseline lengths $L = 1000, 5000, 10000$, and 12000 km. For each baseline length, it is found that $P(\nu_\mu \rightarrow \nu_\mu)$ is more sensitive to $\sin 2\theta_{13}$ at energies around its local maximum while it is more sensitive to $\cos 2\theta_{23}$ at energies around its local minimum. On the other hand, the appearance probability $P(\nu_e \rightarrow \nu_\mu)$ is sensitive to $\sin 2\theta_{13}$ and $\cos 2\theta_{23}$ only near its local maximum. We observe that the θ_{23} degeneracy in $P(\nu_\mu \rightarrow \nu_\mu)$ is absent at energies around the local maximum of this probability, provided θ_{13} is sufficiently large. The θ_{23} degeneracy is also absent in general near the local maximum of $P(\nu_e \rightarrow \nu_\mu)$. Using analytic approximations for neutrino oscillation probabilities, we demonstrate that the above observations for $L = 1000, 5000, 10000$, and 12000 km are in fact valid for all distances. The implications of these results on probing the octant of θ_{23} are discussed in details.

PACS numbers: 14.60.Pq, 13.15.+g, 14.60.Lm

* E-mail: glin@cc.nctu.edu.tw

† E-mail: umeda@faculty.nctu.edu.tw

I. INTRODUCTION

The understanding of neutrino masses and mixing matrix is crucial to unveil the mystery of lepton flavor structures. The updated SK analysis of the atmospheric neutrino data gives [1]

$$1.5 \cdot 10^{-3} \text{ eV}^2 < |\Delta m_{31}^2| < 3.4 \cdot 10^{-3} \text{ eV}^2, \sin^2 2\theta_{23} > 0.92. \quad (1)$$

This is a 90% C.L. range with the best fit values given by $\sin^2 2\theta_{23} = 1$ and $\Delta m_{31}^2 = 2.1 \cdot 10^{-3} \text{ eV}^2$ respectively. An earlier result based upon L/E analysis gives [2]

$$1.9 \cdot 10^{-3} \text{ eV}^2 < |\Delta m_{31}^2| < 3.0 \cdot 10^{-3} \text{ eV}^2, \sin^2 2\theta_{23} > 0.9. \quad (2)$$

at 90% C.L. where the best fit values are given by $\sin^2 2\theta_{23} = 1$ and $\Delta m_{31}^2 = 2.4 \cdot 10^{-3} \text{ eV}^2$ respectively. The scenario of $\nu_\mu \rightarrow \nu_\tau$ oscillation for atmospheric neutrinos has been confirmed by the K2K experiment [3, 4]. Furthermore the results in the solar neutrino oscillation measurements are also confirmed by KamLAND reactor measurements [5, 6]. Combining these measurements, the LMA solution of the solar neutrino problem is established and the updated 2σ parameter ranges are given by [7]

$$7.21 \cdot 10^{-5} \text{ eV}^2 < \Delta m_{21}^2 < 8.63 \cdot 10^{-5} \text{ eV}^2, 0.267 < \sin^2 \theta_{12} < 0.371, \quad (3)$$

with the best fit values $\Delta m_{21}^2 = 7.92 \cdot 10^{-5} \text{ eV}^2$ and $\sin^2 \theta_{12} = 0.314$.

Despite the achievements so far in measuring the neutrino mixing parameters, the sign of Δm_{31}^2 , the mixing angle θ_{13} and the CP violating parameter δ_{CP} in the mixing matrix remain to be determined. Furthermore, one is keen to resolve the octant degeneracy of θ_{23} [8].

The mixing angle θ_{13} is constrained by the reactor experiments [9, 10]. The CHOOZ experiment [9] gives a more stringent constraint on θ_{13} with $\sin^2 2\theta_{13} < 0.1$ for a large Δm_{31}^2 (90% C.L.). A recent global fit based upon three-flavor neutrino oscillation gives the 2σ upper bound, $\sin^2 2\theta_{13} < 0.124$ [7]. It is well known that the mixing angle θ_{13} can be enhanced by the matter effect in Earth. The appearance oscillations $\nu_\mu \rightarrow \nu_e$, $\nu_e \rightarrow \nu_\mu$, and the survival mode $\nu_\mu \rightarrow \nu_\mu$ performed in a very-long baseline have been proposed [11] to probe the angle θ_{13} and the sign of Δm_{31}^2 . Furthermore, the aforementioned very long baseline neutrino experiments as well as future atmospheric neutrino experiments are proposed to determine the deviation of θ_{23} to maximality [12]. In this work, we focus on

the mixing angle θ_{23} . We shall provide a global survey on ideal neutrino energies in the GeV range and baseline lengths from 10^3 km to 10^4 km for probing the octant of the mixing angle θ_{23} . The muon neutrino survival probability $P(\nu_\mu \rightarrow \nu_\mu) \equiv P_{\mu\mu}$ and electron neutrino appearance probability $P(\nu_e \rightarrow \nu_\mu) \equiv P_{e\mu}$ are both studied for this purpose. We observe that the muon neutrino survival probability $P_{\mu\mu}$ has complementary dependencies on mixing angles θ_{13} and θ_{23} as the neutrino energy varies. This property is established by studying the dependencies of $P_{\mu\mu}$ on $\cos 2\theta_{23}$ and $\sin 2\theta_{13}$ while keeping other parameters fixed. The choice of the parameter $\cos 2\theta_{23}$ is appropriate as

$$\frac{1}{2} \cos 2\theta_{23} = \frac{1}{2} - \sin^2 \theta_{23}, \quad (4)$$

which is a probe to the deviation of θ_{23} to the best-fit value $\pi/4$. We find that the dependencies of $P_{\mu\mu}$ on $\cos 2\theta_{23}$ and $\sin 2\theta_{13}$ at energies near local maxima of this probability differ drastically from those at energies near local minima of the same probability. In the former case, the probability $P_{\mu\mu}$ is always more sensitive to $\sin 2\theta_{13}$. Furthermore, the θ_{23} degeneracy is absent in this case. In the latter case, the probability $P_{\mu\mu}$ is more sensitive to $\cos 2\theta_{23}$ while the θ_{23} degeneracy is generally present. Such information is useful for probing the octant of θ_{23} . We also study sensitivities of the probability $P_{e\mu}$ to $\cos 2\theta_{23}$ and $\sin 2\theta_{13}$ with other parameters fixed. We only focus on energies near the local maximum of $P_{e\mu}$ as this probability is not sensitive to mixing parameters for energies near its local minimum.

This paper is organized as follows. In Section II, we compare results on the oscillation probability $P_{e\mu}$ obtained by the full calculation with those obtained by various analytic approximations. This comparison is essential since analytic approximations will be employed for discussions in later sessions. To set up the analytic approximation, we introduce the concept of average density which varies with the total neutrino path-length inside the Earth. Applying full calculations and the two-layer analytic approximations [13], we identify the energy values for local maxima and local minima of neutrino oscillation probabilities $P_{\mu\mu}$ and $P_{e\mu}$ for baseline lengths $1000 \leq L/\text{km} \leq 12000$. It is found that the two-layer approximation is quite satisfactory compared to the full calculation for computing these energy values. In Section III, we first present the dependencies of $P_{\mu\mu}$ and $P_{e\mu}$ on the CP violation phase δ_{CP} . It will be shown that, unlike $P_{e\mu}$, $P_{\mu\mu}$ is not sensitive to the CP violation phase δ_{CP} . We study numerically the effect of CP violation phase to the appearance probability $P_{e\mu}$. The result confirms the so-called magic baseline [14, 15, 16] at $L \approx 7600$ km where $P_{e\mu}$ is

rather insensitive to the CP violation phase. After discussions on the CP violation phase, we present the contour graphs of probabilities $P_{\mu\mu}$ and $P_{e\mu}$ on $\cos 2\theta_{23} - \sin 2\theta_{13}$ plane for baseline lengths $L = 1000, 5000, 10000$, and 12000 km. At all these baseline lengths, we shall see that $P_{\mu\mu}$ is more sensitive to $\sin 2\theta_{13}$ at energies around its local maximum while it is more sensitive to $\cos 2\theta_{23}$ at energies around its local minimum. Such observations are then justified by using the two-layer analytic approximations for neutrino oscillation probabilities. With this approximation, the baseline lengths and neutrino energies allowing an unambiguous determination of θ_{23} through measuring $P_{\mu\mu}$ are identified. In Section IV, we discuss the prospects of probing the θ_{23} octant via measuring $P_{e\mu}$ and $P_{\mu\mu}$. We then conclude in the same section.

II. THE COMPARISON OF FULL CALCULATIONS AND ANALYTIC APPROXIMATIONS

We begin the discussions with the relation connecting flavor and mass eigenstates of neutrinos, $\nu_\alpha = \sum_i U_{\alpha i} \nu_i$, with U the Maki-Nakagawa-Sakata mixing matrix [17] given by

$$U = \begin{pmatrix} c_{12}c_{13} & s_{12}c_{13} & s_{13}e^{-i\delta_{\text{CP}}} \\ -s_{12}c_{23} - c_{12}s_{13}s_{23}e^{i\delta_{\text{CP}}} & c_{12}c_{23} - s_{12}s_{13}s_{23}e^{i\delta_{\text{CP}}} & c_{13}s_{23} \\ s_{12}s_{23} - c_{12}s_{13}c_{23}e^{i\delta_{\text{CP}}} & -c_{12}s_{23} - s_{12}s_{13}c_{23}e^{i\delta_{\text{CP}}} & c_{13}c_{23} \end{pmatrix}, \quad (5)$$

where s_{ij} and c_{ij} denote $\sin \theta_{ij}$ and $\cos \theta_{ij}$, respectively. The value for the Dirac type CP-phase δ_{CP} ranges from 0 to 2π . The evolutions of neutrino flavor eigenstates are governed by the equation

$$i \frac{d}{dt} |\nu(t)\rangle = \left\{ \frac{1}{2E_\nu} U \begin{pmatrix} 0 & 0 & 0 \\ 0 & \Delta m_{21}^2 & 0 \\ 0 & 0 & \Delta m_{31}^2 \end{pmatrix} U^\dagger + \begin{pmatrix} V & 0 & 0 \\ 0 & 0 & 0 \\ 0 & 0 & 0 \end{pmatrix} \right\} |\nu(t)\rangle, \quad (6)$$

where $|\nu(t)\rangle = (\nu_e(t), \nu_\mu(t), \nu_\tau(t))^T$, $\Delta m_{ij}^2 \equiv m_i^2 - m_j^2$ is the mass-squared difference between the i -th and j -th mass eigenstates, and $V \equiv \sqrt{2}G_F N_e$ is the effective potential arising from the charged current interaction between ν_e and electrons in the medium with N_e the electron number density. Numerically $V = 7.56 \times 10^{-14} (\rho/[\text{g}/\text{cm}^3]) Y_e [\text{eV}]$ with Y_e denoting the number of electrons per nucleon. We take $Y_e \sim 0.5$ in our calculations. One solves Eq. (6) by diagonalizing the Hamiltonian on its right hand side. This amounts to writing

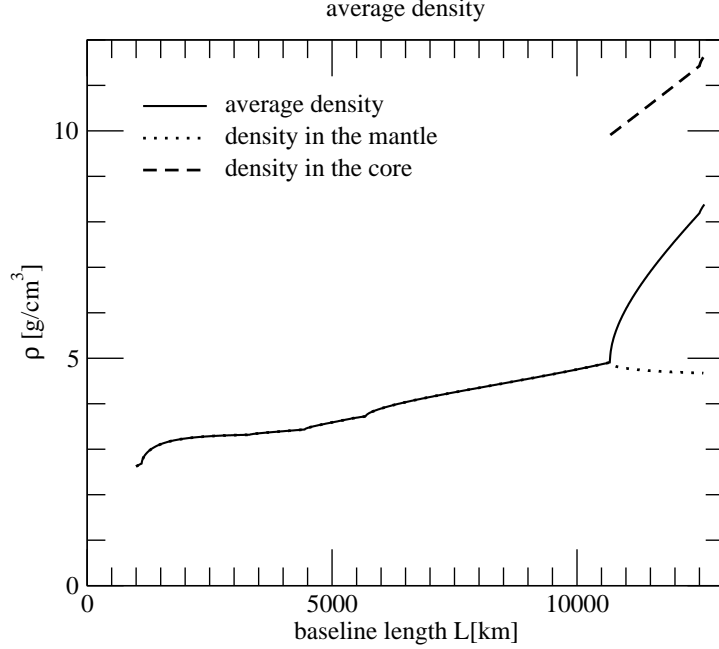


FIG. 1: The average Earth density along the path traversed by the neutrino as a function of the path length L .

the right hand side of Eq. (6) as $U'H'U'^{\dagger}|\nu(t)\rangle$ with U' the neutrino mixing matrix in the matter and $H' \equiv \text{diag}(E_1, E_2, E_3)$ the Hamiltonian after diagonalization. To obtain various oscillation probabilities described later, we have used the parametrization in [18] for the Earth density profile.

For analytic calculations, we employ the two-layer approximation for the Earth density profile [13]. Given a path-length L for a neutrino traversing the Earth medium, one can divide L into the sum $L = L_1 + L_2 + \cdots L_n$ with each L_i corresponding to a region with a specific matter density. The average density for this path-length is then given by $\rho = (\rho_1 L_1 + \rho_2 L_2 + \cdots \rho_n L_n)/L$. The Earth medium can be categorized as the Earth mantle and the Earth core. If a neutrino only traverses the Earth mantle, we shall use the one-density approximation for the analytic calculation with the density defined by the above prescription. However, if a neutrino traverses both the Earth mantle and the Earth core, one should write the total neutrino path-length as $L = 2L_m + L_c$ with

$$\begin{aligned}
 L_m &= R \left(\cos \theta_n - \sqrt{\frac{r_c^2}{R^2} - \sin^2 \theta_n} \right), \\
 L_c &= 2R \sqrt{\frac{r_c^2}{R^2} - \sin^2 \theta_n},
 \end{aligned} \tag{7}$$

where $R = 6371$ km and $r_c = 3480$ km are the radii of the entire Earth and the Earth core respectively while θ_n is the incident Nadir angle of the neutrino. We note that the critical Nadir angle for a neutrino to pass the Earth core is 33.17° corresponding to $L = 10674$ km. For $L > 10674$ km, one separately defines average densities within the path-length L_m and the path-length L_c respectively. The average densities as functions of the neutrino path-length is shown in Fig. 1. For $L \leq 10674$ km, there is only one curve for the average density, which is represented by the solid line in the figure. Beyond this distance, one can define the average density in the core and the average density in the mantle, which are represented by dashed and dotted lines respectively. Alternatively, one can also define single average density for $L > 10674$ km by ignoring the distinction between the mantle and the core. This is seen from the solid line for $L > 10674$ km. However, in our analytic calculations, we shall adopt the two-density approach for $L > 10674$ km.

For analytic calculations, we only compute oscillation probabilities up to the lowest order in $\tau \equiv \Delta m_{21}^2 / \Delta m_{31}^2$. In other words, we set $\Delta m_{21}^2 = 0$ in analytic calculations and consequently the mixing angle θ_{12} and the CP phase δ_{CP} drop out from the oscillation probabilities. The probabilities $P_{\mu\mu}$ and $P_{e\mu}$ in the two-layer approximations are given by [19, 20, 21, 22, 23]:

$$\begin{aligned} P_{\mu\mu} &= \cos^4 \theta_{23} + (u^2 + v^2) \sin^4 \theta_{23} + 2 \cos^2 \theta_{23} \sin^2 \theta_{23} (u \cos t + v \sin t), \\ P_{e\mu} &= \sin^2 \theta_{23} (1 - u^2 - v^2). \end{aligned} \quad (8)$$

The quantities u , v and t are defined as

$$\begin{aligned} u &= \cos(2\phi^m) \cos(\phi^c) - \cos(2\theta_{13}^c - 2\theta_{13}^m) \sin(2\phi^m) \sin(\phi^c), \\ v &= -\cos(2\theta_{13}^m) [\sin(\phi^c) \cos(2\phi^m) \cos(2\theta_{13}^c - 2\theta_{13}^m) + \cos(\phi^c) \sin(2\phi^m)] \\ &\quad + \sin(2\theta_{13}^m) \sin(\phi^c) \sin(2\theta_{13}^c - 2\theta_{13}^m), \\ t &= \frac{(M_{13}^2)^m + (m_{13}^2)^m}{4E} \times 2L^m + \frac{(M_{13}^2)^c + (m_{13}^2)^c}{4E} \times L^c, \end{aligned} \quad (9)$$

where

$$\begin{aligned} \phi^{m(c)} &= \frac{\Delta_{31}^{m(c)}}{4E} L^{m(c)}, \\ (M_{13}^2)^{m(c)} &= (\Delta m_{31}^2 + A_e^{m(c)} + \Delta_{31}^{m(c)})/2, \\ (m_{13}^2)^{m(c)} &= (\Delta m_{31}^2 + A_e^{m(c)} - \Delta_{31}^{m(c)})/2, \end{aligned} \quad (10)$$

with

$$\Delta_{31}^{m(c)} = \sqrt{(\Delta m_{31}^2 \sin 2\theta_{13})^2 + (A_e^{m(c)} - \Delta m_{31}^2 \cos 2\theta_{13})^2}. \quad (11)$$

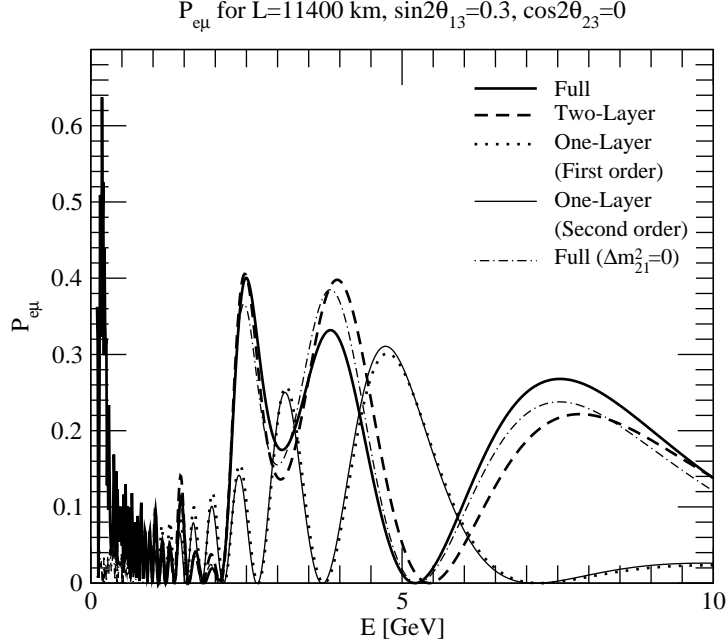


FIG. 2: A comparison of $P_{e\mu}$ obtained by the full numerical calculation and various approximations. The thick solid curve denotes the result by the full numerical calculation. The dotted-dashed curve denotes the result by setting $\Delta m_{21}^2 = 0$ in the full numerical calculation. The dashed curve represents the result obtained by the two-layer approximation in the leading order of $\tau \equiv \Delta m_{21}^2 / \Delta m_{31}^2$. The dotted curve denotes the result obtained by one-density approximation in the leading order of τ while the thin solid curve is that obtained by the one-density approximation in the next-to-leading order of τ .

The superscripts m and c denote quantities defined in the Earth mantle and the Earth core respectively. For neutrinos traversing only the Earth mantle, one simply sets $L_c = 0$, $2L_m = L$ in the above equations and recovers well known expressions for $P_{\mu\mu}$ and $P_{e\mu}$ in the one-density approximation [24].

The accuracy of two-layer approximation is shown in Fig. 2 with a comparison of this approximation to the full numerical calculation and other approximations. In the calculations, we have assumed the normal mass hierarchy and taken $\sin 2\theta_{13} = 0.3$, $\cos 2\theta_{23} = 0$, $\delta_{\text{CP}} = 0$, $\Delta m_{31}^2 = 2.4 \times 10^{-3} \text{ eV}^2$, $\Delta m_{21}^2 = 8.2 \times 10^{-5} \text{ eV}^2$, and $\tan^2 \theta_{12} = 0.39$ [25]. This set of parameters will be adopted for later calculations unless specific mentioning of other choices. This set of parameters differ from the most updated best-fit values quoted right after Eq. (3). However, both set of parameters give undistinguishable results on $P_{e\mu}$ and $P_{\mu\mu}$.

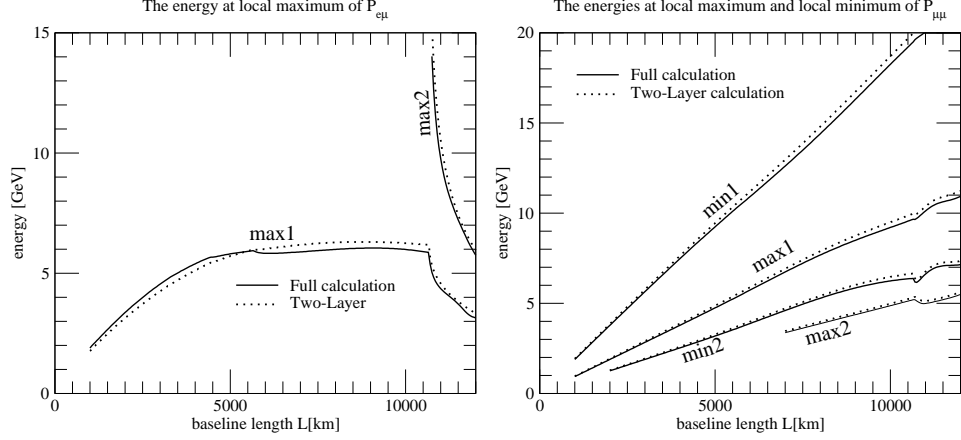


FIG. 3: Left panel: the energy at the local maximum of $P_{e\mu}$, as a function of L . Right panel: energies at local maxima and local minima of $P_{\mu\mu}$, as functions of L .

in the energy range concerned here. A comparison made at $L = 11400$ km has two purposes. First of all, it is known that the series expansion in the parameter τ is valid for $L/E_\nu \ll 10^4$ (km/GeV) [24, 26]. Hence analytic calculations performed at this baseline length test the marginal region of the condition $L/E_\nu \ll 10^4$ (km/GeV). Secondly this path-length implies that the neutrino traverses both the Earth mantle and the Earth core. Therefore it is also a good test to the two-layer approximation. It is seen that the two-layer approximation, unlike the one-layer approximation, reproduces well the peak energies of $P_{e\mu}$, while it gives peak probabilities deviating from those obtained from the full calculation by 15% – 20%. We also see that the two-layer approximation agrees well with the full calculation in the limit $\Delta m_{21}^2 = 0$.

For later analysis, we compute energies at local maxima of $P_{e\mu}$ and those at local maxima and local minima of $P_{\mu\mu}$ for the baseline range $1000 \leq L/\text{km} \leq 12000$. The results are depicted in Fig. 3. We do not study local minima of $P_{e\mu}$ since their values are not sensitive to mixing angles θ_{13} and θ_{23} . It is seen that the analytic approximation is satisfactory for computing energies at local maxima and local minima of neutrino oscillation probabilities. We point out that the energy curves in Fig. 3 are calculated with $\sin 2\theta_{13} = 0.3$ and $\cos 2\theta_{23} = 0$. It is found that these curves are not sensitive to the values of $\sin 2\theta_{13}$ and $\cos 2\theta_{23}$.

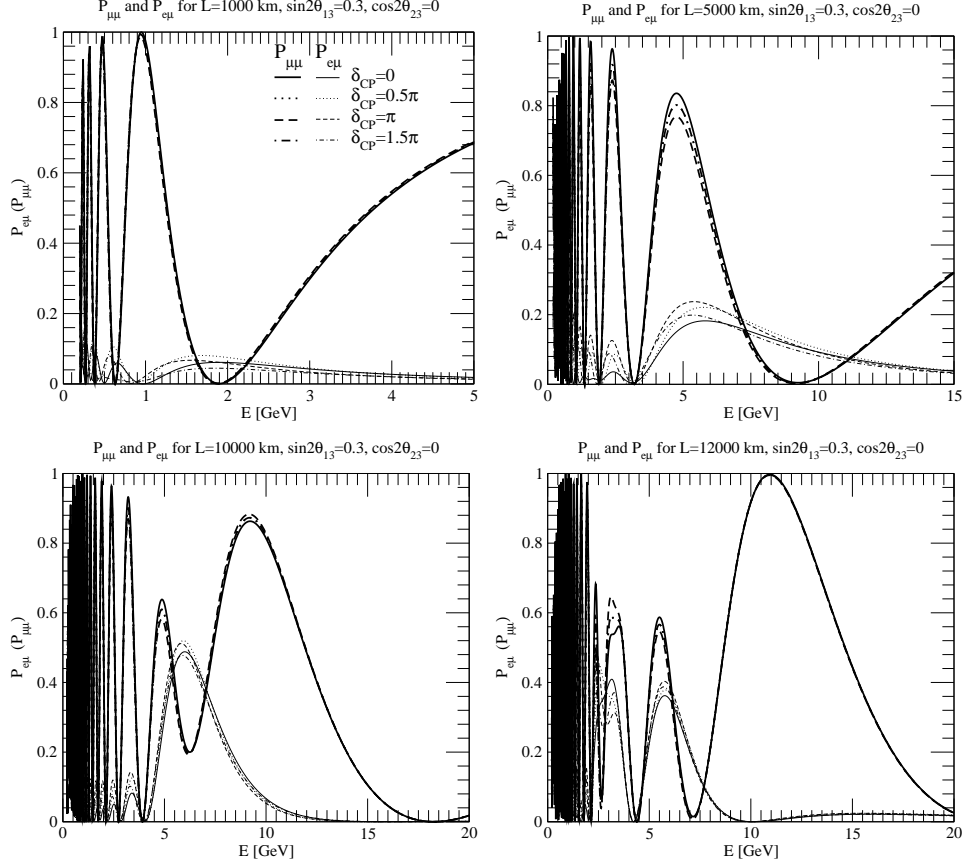


FIG. 4: The CP phase dependencies of $P_{\mu\mu}$ and $P_{e\mu}$ for $L = 1000$ km, 5000 km, 10000 km and 12000 km respectively. The probability $P_{\mu\mu}$ is described by the thick curve while $P_{e\mu}$ is described by the thin curve.

III. CONDITIONS FOR THE ABSENCE OF θ_{23} DEGENERACY IN $P_{\mu\mu}$ AND $P_{e\mu}$ AT DIFFERENT ENERGIES

A. The dependencies of $P_{\mu\mu}$ and $P_{e\mu}$ on δ_{CP}

Before concentrating on θ_{13} and θ_{23} dependencies of neutrino oscillation probabilities, we first study the CP phase dependencies with the full numerical calculations. It is easily seen from Fig. 4 that $P_{\mu\mu}$ is not sensitive to the CP phase for all distances displayed. On the other hand, $P_{e\mu}$ is rather sensitive to the CP phase for $L = 1000$ km and 5000 km. In order to quantify the CP phase dependence of $P_{e\mu}$, we study peak values of $P_{e\mu}$, which occur at energies described by the curve **max1** in Fig. 3 for different baseline lengths. This peak value for a specific baseline length depends on the CP violation phase δ_{CP} and we

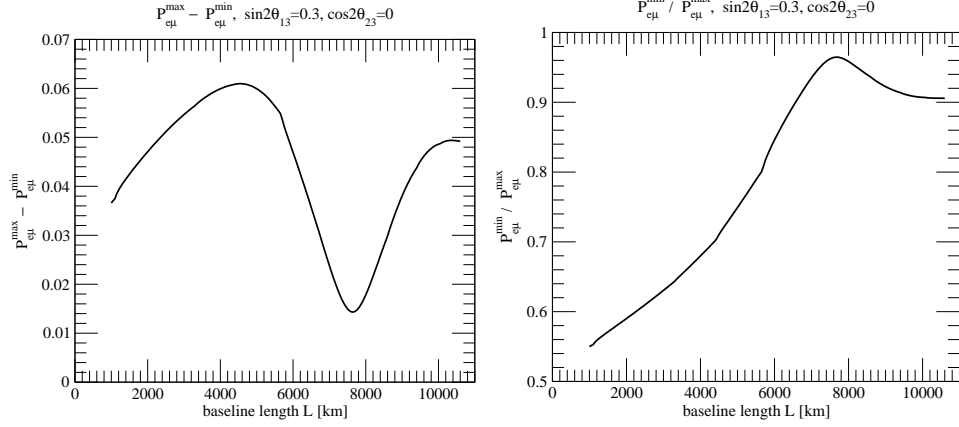


FIG. 5: The difference and the ratio of $P_{e\mu}^{\max}$ and $P_{e\mu}^{\min}$ as functions of the baseline length.

denote the maximum and the minimum of this value as $P_{e\mu}^{\max}$ and $P_{e\mu}^{\min}$ respectively. The difference and the ratio of these two values as functions of the baseline length L are shown in Fig. 5. It is interesting to note that the ratio $P_{e\mu}^{\min}/P_{e\mu}^{\max}$ increases monotonically with the baseline length until $L = 7600$ km. The ratio begins to decrease for a larger baseline but remains larger than 90%. In fact, one can see that $P_{e\mu}^{\max}$ and $P_{e\mu}^{\min}$ differ by less than 10% for $L \geq 6500$ km. We point out that $1 - P_{e\mu}^{\min}/P_{e\mu}^{\max}$ reaching to minimum at $L = 7600$ km confirms the so-called magic baseline for the probability $P_{e\mu}$ [14, 15, 16].

B. The dependencies of $P_{\mu\mu}$ and $P_{e\mu}$ on mixing angles θ_{13} and θ_{23}

Having studied CP phase dependencies of oscillation probabilities, we now focus on θ_{13} and θ_{23} dependencies. In this study we set the CP phase δ_{CP} equal to zero. The results are presented in Fig. 6. It is easily seen that the values of $P_{\mu\mu}$ at its local maximum and local minimum depend on mixing angles θ_{13} and θ_{23} while only the local maximum of $P_{e\mu}$ depends on these parameters. This confirms our earlier comments concerning the left panel of Fig. 3. We point out that the differences between solid and dotted curves in Fig. 6 reflect the effect of $\sin 2\theta_{13}$; while the differences between solid and dashed curves there reflect the effect of $\cos 2\theta_{23}$.

We now present contour graphs of $P_{\mu\mu}$ and $P_{e\mu}$ on the $\cos 2\theta_{23} - \sin 2\theta_{13}$ plane. The range for $\cos 2\theta_{23}$ is chosen such that $\sin 2\theta_{23} > 0.9$ [2], i.e., $-0.316 < \cos 2\theta_{23} < 0.316$; while $\sin^2 2\theta_{13}$ is chosen to be less than 0.1, i.e., $\sin 2\theta_{13} < 0.316$. The contour graphs of $P_{\mu\mu}$ at

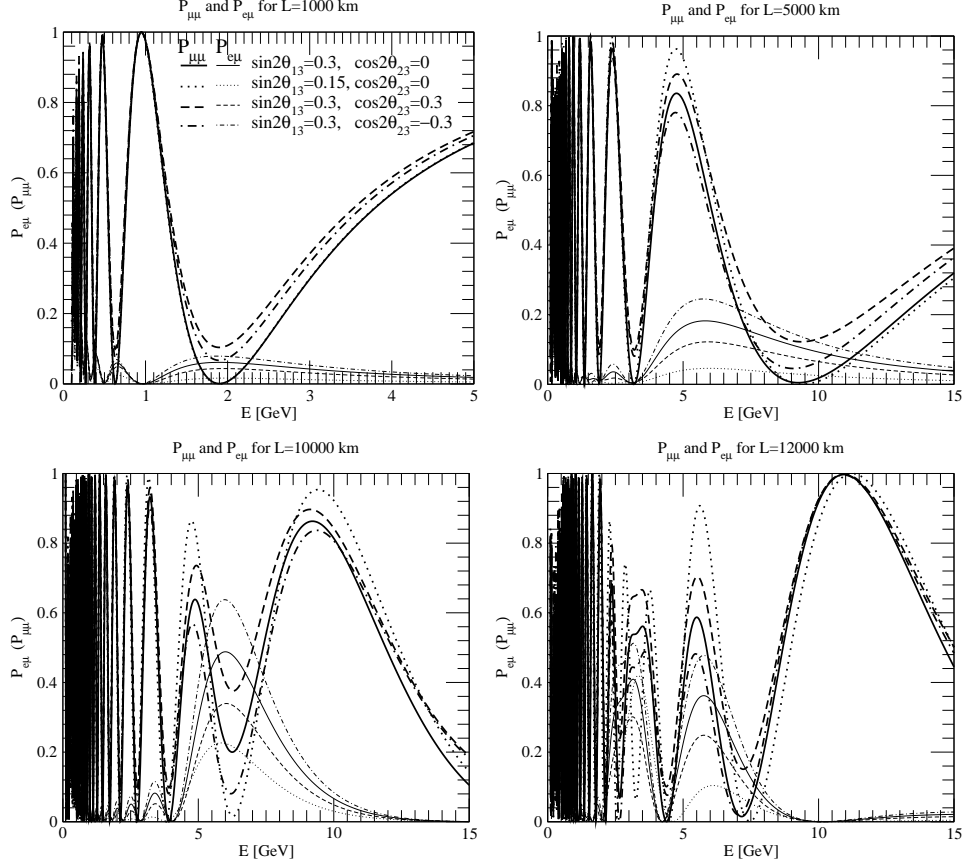


FIG. 6: The θ_{13} and θ_{23} dependencies of $P_{\mu\mu}$ and $P_{e\mu}$ for $L = 1000$ km, 5000 km, 10000 km and 12000 km respectively. The probability $P_{\mu\mu}$ is described by the thick curve while $P_{e\mu}$ is described by the thin curve.

different baseline lengths are presented in Fig. 7. Except for $L = 1000$ km, we have shown contours of $P_{\mu\mu}$ for energies in the vicinity of both local maximum and local minimum of this probability. The contour for the local maximum of $P_{\mu\mu}$ at $L = 1000$ km is not shown since $P_{\mu\mu}$ at this energy and baseline length is not sensitive to mixing angles θ_{13} and θ_{23} . For $L = 5000$ km, 10000 km and 12000 km, it is seen that the contours at local maxima of $P_{\mu\mu}$ and those at local minima of $P_{\mu\mu}$ behave rather differently. The former are in general more parallel to the $\cos 2\theta_{23}$ -axis while the latter are generally more parallel to the $\sin 2\theta_{13}$ -axis. We note that the local maximum (**max2**) of $P_{\mu\mu}$ at $L = 12000$ km can vary from 0.9 to a much smaller value, 0.45, which is a result of significant matter effects. Similarly, due to large matter effects, the local minimum (**min2**) of $P_{\mu\mu}$ at $L = 10000$ km can vary from 0 to a much larger value, 0.4. We also notice that, at this baseline length, the θ_{23} degeneracy

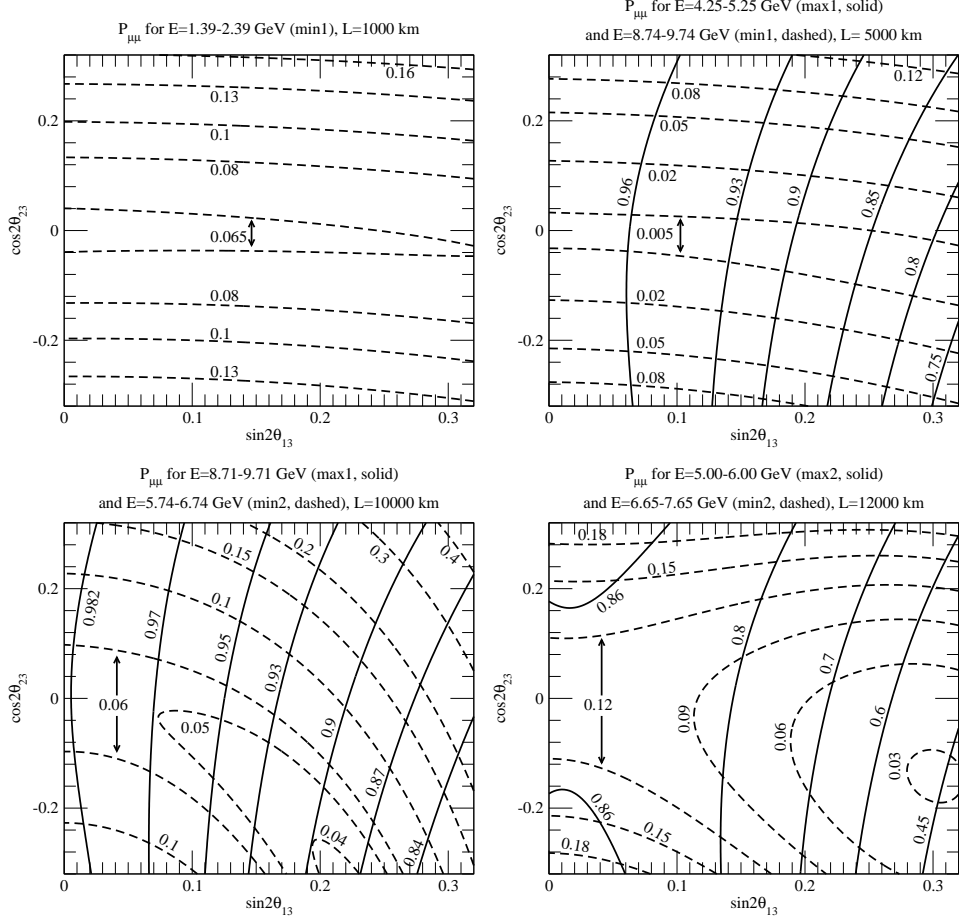


FIG. 7: The contour graphs of the muon neutrino survival probability $P_{\mu\mu}$ on the $\cos 2\theta_{23} - \sin 2\theta_{13}$ plane. At $L = 1000$ km, the local minimum of $P_{\mu\mu}$ on the curve **min1** occurs at $E = 1.89$ GeV. We plot the contour graph of $P_{\mu\mu}$ by averaging this probability over an 1 GeV energy range centered at the above local minimum. At $L = 5000$ km, the local maximum of $P_{\mu\mu}$ on the curve **max1** occurs at $E = 4.75$ GeV while the local minimum of this probability on the curve **min1** occurs at $E = 9.24$ GeV. We plot the contour graphs of $P_{\mu\mu}$ in the energy range $4.25 \leq E/\text{GeV} \leq 5.25$ for the former case and $8.74 \leq E/\text{GeV} \leq 9.74$. The same type of convention applies to $L = 10000$ km and 12000 km.

is absent for $P_{\mu\mu} > 0.1$. In general, such a degeneracy is also absent for energies near local maxima of $P_{\mu\mu}$. However, the probabilities are not sensitive to $\cos 2\theta_{23}$ in those cases. For comparisons, we also present contour graphs for the appearance probability $P_{e\mu}$ at different baseline lengths. It is clearly seen that $P_{e\mu}$ is only sensitive to $\sin 2\theta_{13}$ for most cases. The sensitivity to $\cos 2\theta_{23}$ only occurs at very long baseline lengths and large values of $\sin 2\theta_{13}$.

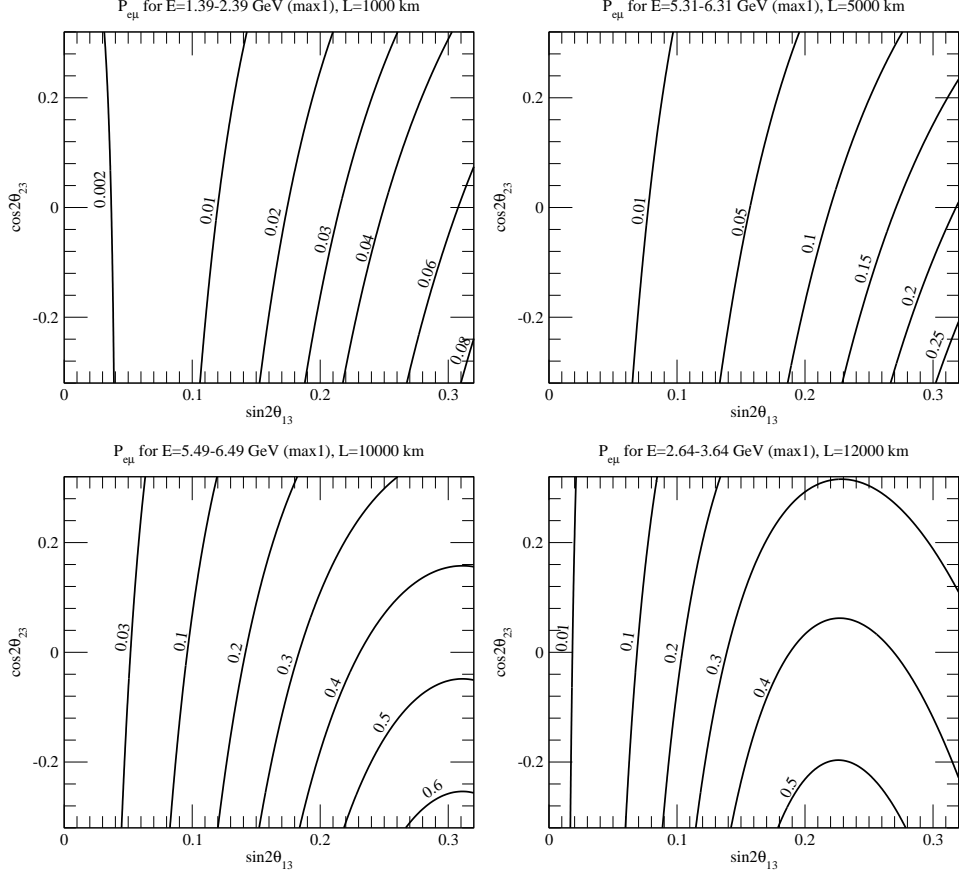


FIG. 8: The contour graphs for the oscillation probability $P_{e\mu}$ on the $\cos 2\theta_{23} - \sin 2\theta_{13}$ plane. We plot contours of $P_{e\mu}$ at energies near the local maximum (**max1**) of this probability.

For example, at $L = 10000$ km, $P_{e\mu}$ becomes sensitive to $\cos 2\theta_{23}$ as $\sin 2\theta_{13}$ approaches 0.3. At $L = 12000$ km, $P_{e\mu}$ becomes sensitive to $\cos 2\theta_{23}$ when $\sin 2\theta_{13}$ is greater than 0.2.

C. A global look at the absence of θ_{23} degeneracy

In this subsection, we focus on θ_{23} dependencies of $P_{\mu\mu}$ and $P_{e\mu}$ for general baseline lengths. The two-layer analytic approximations for $P_{\mu\mu}$ and $P_{e\mu}$ will be employed for our discussions, and observations in the previous subsection shall be justified. It is instructive to rewrite Eq. (8) in polynomials of $\cos 2\theta_{23}$:

$$\begin{aligned} f(y, z) &= -\alpha y^2 + (\alpha + \beta)y + (1 - \beta), \\ g(y, z) &= -\gamma(y - 1), \end{aligned} \tag{12}$$

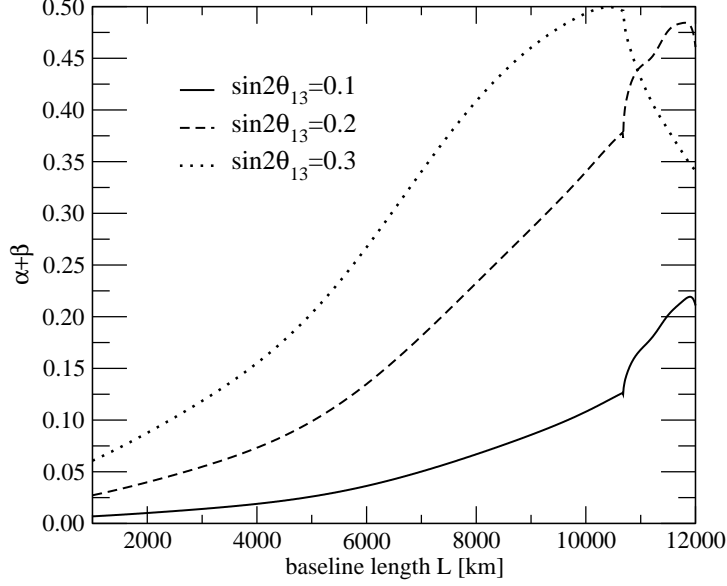


FIG. 9: The coefficient $\alpha(z) + \beta(z)$ calculated along the energy curve **max1** in the left panel of Fig. 3. The values of $\sin 2\theta_{13}$ are taken to be 0.1, 0.2 and 0.3 respectively.

with $f(y, z) \equiv P_{\mu\mu}$, $g(y, z) \equiv P_{e\mu}$, $y \equiv \cos 2\theta_{23}$ and $z \equiv \sin 2\theta_{13}$. Furthermore,

$$\begin{aligned}\alpha &= -\frac{1}{4} [(u - \cos t)^2 + (v - \sin t)^2], \\ \beta &= \frac{1}{2} (1 - u^2 - v^2) + \frac{1}{4} [(u - \cos t)^2 + (v - \sin t)^2], \\ \gamma &= \frac{1}{2} (1 - u^2 - v^2).\end{aligned}\tag{13}$$

We note that the $\sin 2\theta_{13}$ dependencies of $P_{\mu\mu}$ and $P_{e\mu}$ reside in quantities u , v , $\cos t$ and $\sin t$. These quantities also depend on the baseline length L and the neutrino energy E . Hence the coefficients α , β and γ also depend on the baseline length L and the neutrino energy E . It is interesting to note that $\alpha + \beta = \gamma$. Therefore we have

$$P_{\mu\tau} = \alpha (y^2 - 1),\tag{14}$$

using $P_{\mu e} + P_{\mu\mu} + P_{\mu\tau} = 1$ and $P_{\mu e} = P_{e\mu}$ with our choice of $\delta_{\text{CP}} = 0$. The contour structure of $P_{e\mu}$ is straightforward as $g(y, z)$ is only a linear function of y . Hence no θ_{23} degeneracy presents in the contour graphs depicted in Fig. 8. Additionally, the sensitivity of $P_{e\mu}$ to $\cos 2\theta_{23}$ is $dg(y, z)/dy = -(\alpha(z) + \beta(z))$. The coefficient $\alpha + \beta$ evaluated along the energy curve **max1** in the left panel of Fig. 3 are plotted in Fig. 9 for $\sin 2\theta_{13} = 0.1$, 0.2 and 0.3. For $\sin 2\theta_{13} = 0.3$, $\alpha + \beta$ reaches to the maximal value, 0.5, for $L \simeq 10500$ km. For $\sin 2\theta_{13} = 0.1$

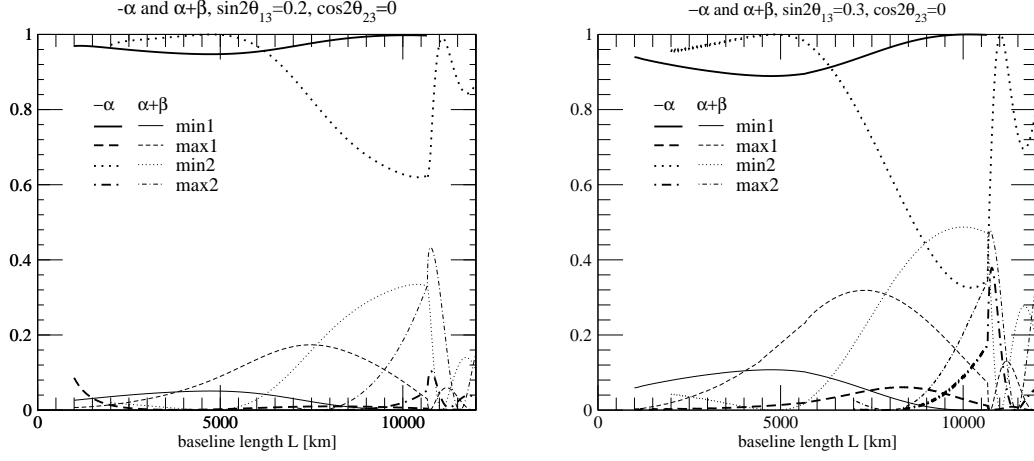


FIG. 10: The coefficients $-\alpha$ and $\alpha + \beta$ evaluated along energy curves in the right panel of Fig. 3. The coefficients are calculated with $\sin 2\theta_{13} = 0.2$ and 0.3 on the left and right panels respectively. The thick curves denote values of $-\alpha$ while thin curves denote those of $\alpha + \beta$. For solid and dotted curves, the thick curves generally dominate over the corresponding thin ones. For dashed and dotted-dashed curves, the thin curves generally dominate over the thick ones.

and 0.2 , $\alpha + \beta$ rises quickly as the baseline length L surpasses 10674 km. We note that the value of $P_{e\mu}$ is proportional to $\alpha + \beta$. Hence $\alpha + \beta$ shown in Fig. 9 is its own maximal value for each baseline length L .

The contour structure of $P_{\mu\mu}$ can be analyzed through the quadratic polynomial $f(y, z)$ in y . If $-\alpha \gg \alpha + \beta$, generally there are two solution curves for $f(y, z) = p$ compatible with the ranges of y and z where p is a given value for $P_{\mu\mu}$. Let us suppose that $z \equiv \sin 2\theta_{13}$ is measured in the future [27, 28] with a central value z_0 . The two solution curves for the equation $f(y, z) = p$ then intersect with the straight line $z \equiv \sin 2\theta_{13} = z_0$ at two points (y_1, z_0) and (y_2, z_0) . This is actually what we have seen in Fig. 7 for local minima of $P_{\mu\mu}$. If, on the other hand, $-\alpha \simeq \alpha + \beta$ or even $-\alpha \ll \alpha + \beta$, there exists only one solution curve for the equation $f(y, z) = p$. This is because that the two points (y_1, z_0) and (y_2, z_0) can not simultaneously satisfy the constraint $-0.316 < y < 0.316$ since $|y_1 + y_2| = -(\alpha + \beta)/\alpha \geq 1$. This is actually what we have seen in Fig. 7 for local maxima of $P_{\mu\mu}$. To justify this observation, it remains to show that the coefficient $-\alpha$ dominates over $\alpha + \beta$ at energies corresponding to local minima of $P_{\mu\mu}$ while the latter dominates over the former at energies corresponding to local maxima of $P_{\mu\mu}$. This is clearly demonstrated in Fig. 10 where the

coefficients $-\alpha$ and $\alpha + \beta$ are evaluated along energy curves in the right panel of Fig. 3. We have calculated the coefficients with $\cos 2\theta_{23} = 0$ and $\sin 2\theta_{13} = 0.2, 0.3$ respectively. We remark that other choices for $\cos 2\theta_{23}$ do not produce noticeable changes on the energy curves where $-\alpha$ and $\alpha + \beta$ are evaluated.

It is easily seen that $\alpha + \beta$ always dominates over $-\alpha$ when these coefficients are evaluated at energies along **max1** or **max2** in the right panel of Fig. 3. In such cases, the θ_{23} degeneracy is absent in the solutions of $f(y, z) = p$. Namely there exists only one solution curve for the above equation. Reversely, $-\alpha$ always dominates over $\alpha + \beta$ when these coefficients are evaluated at energies along **min1**. The situation is slightly more complicated when these coefficients are evaluated at energies along **min2**. In this case $-\alpha$ no longer dominates over $\alpha + \beta$ for baseline lengths around 10^4 km. In fact, with $\sin 2\theta_{13} = 0.3$, $\alpha + \beta$ is even larger than $-\alpha$ for $9000 \leq L/\text{km} \leq 10500$. This explains the contour structure of $P_{\mu\mu}$ at $L = 10000$ km (see Fig. 7) where the straight line $z = 0.3$ only intersects one equal probability curve $f(y, z = 0.3) = p$. The straight line $z = 0.2$ also behaves the same except for a very small p . We reiterate that the range for $y \equiv \cos 2\theta_{23}$ is $-0.316 < y < 0.316$ due to the constraint $\sin^2 2\theta_{23} > 0.9$ [2]. Therefore, given $z = z_0$, the equation $f(y, z_0) = p$ could have only one solution for y if $-(\alpha(z_0) + \beta(z_0))/\alpha(z_0) > 0.632$. In other words, such values of $-(\alpha(z_0) + \beta(z_0))/\alpha(z_0)$ lead to the absence of θ_{23} degeneracy. In fact, the condition for the absence of θ_{23} degeneracy is even more relaxed. To see this, let us divide our discussions according to the true octant of θ_{23} .

1. **min2**, $\theta_{23} < \pi/4$

Since $\alpha < 0$ and $\alpha + \beta > 0$, the two solutions for y in $f(y, z_0) = p$ are both negative for $1 - \beta(z_0) - p > 0$ while they have opposite signs for $1 - \beta(z_0) - p < 0$. If the true value of θ_{23} is less than $\pi/4$, i.e., the true value of y is positive, then the experimental measurement should give $1 - \beta(z_0) - p < 0$ so that a positive solution for y exists. With $1 - \beta(z_0) - p < 0$, the two solutions for $f(y, z_0) = p$ have opposite signs and the negative solution has a larger absolute value. The negative solution will violate the constraint $-0.316 < y$ if $-(\alpha(z_0) + \beta(z_0))/\alpha(z_0) > 0.316$. For $z_0 = 0.2$, $-(\alpha(z_0) + \beta(z_0))/\alpha(z_0) > 0.316$ is valid for $8300 \leq L/\text{km} \leq 10770$. For $z = 0.3$, the above baseline range is extended to $7410 \leq L/\text{km} \leq 10790$.

2. **min2**, $\theta_{23} > \pi/4$

With a true value of θ_{23} greater than $\pi/4$, i.e., the true value of y less than zero, the value of $1 - \beta(z_0) - p$ can either be positive or negative. The condition $1 - \beta(z_0) - p > (<) 0$ is equivalent to the condition $|y| < (>) (\alpha(z_0) + \beta(z_0)) / (-\alpha(z_0))$. For $-(\alpha(z_0) + \beta(z_0))/\alpha(z_0) > 0.316$, one must have $1 - \beta(z_0) - p > 0$. Hence there exist two negative solutions for y . In this case, the corresponding solutions for θ_{23} are both located in the same octant. For $0.316 < -(\alpha(z_0) + \beta(z_0))/\alpha(z_0) < 0.632$, the spurious solution for y may or may not violate the constraint $y > -0.316$. For $-(\alpha(z_0) + \beta(z_0))/\alpha(z_0) > 0.632$, the spurious solution for y must violate the constraint $y > -0.316$, hence the θ_{23} degeneracy is surely absent. For $\sin 2\theta_{13} = 0.2$, the condition $-(\alpha(z_0) + \beta(z_0))/\alpha(z_0) > 0.632$ can not be achieved along **min2**. For $\sin 2\theta_{13} = 0.3$, the above condition is satisfied for $8270 \leq L/\text{km} \leq 10720$. For $-(\alpha(z_0) + \beta(z_0))/\alpha(z_0) < 0.316$, $1 - \beta(z_0) - p$ can either be positive or negative. For $1 - \beta(z_0) - p > 0$, both solutions for y are negative and satisfying the constraint $y > -0.316$. For $1 - \beta(z_0) - p < 0$, both solutions for y satisfy the constraint $-0.316 < y < 0.316$. However their corresponding θ_{23} angles are situated in different octants.

Let us summarize the results obtained in this subsection. The coefficient $\alpha + \beta$ dominates over $-\alpha$ for energy values along curves **max1** and **max2** for all baseline lengths. Hence the θ_{23} degeneracy is absent along these energy curves for all baseline lengths. The situation along the curve **min1** is just the opposite, the coefficient $-\alpha$ dominates over $\alpha + \beta$ for all baseline lengths. Hence the θ_{23} degeneracy is present for all baseline lengths in this case. The issue of θ_{23} degeneracy becomes more complicated along **min2**, which we have discussed according to the true octant of θ_{23} . Along the energy curve **min2**, the non-degeneracy baseline range is larger for the $\theta_{23} < \pi/4$ case.

IV. DISCUSSIONS AND CONCLUSIONS

We have presented the baselines and energies ideal for probing the octant of θ_{23} through neutrino oscillations. The appearance mode $\nu_e \rightarrow \nu_\mu$ can be studied in a very long baseline with the facility of neutrino factory [29] or the more recent proposed β beam [30]. As said, the sensitivity of $P_{e\mu}$ to θ_{23} is $dg(y, z)/dy = -(\alpha(z) + \beta(z))$ where $g(y, z)$ represents $P_{e\mu}$ in the analytic approximation given by Eq. (12). The maximal value of $\alpha + \beta$ for each baseline

length is shown in Fig. 9. At the magic baseline, $L = 7600$ km, $\alpha + \beta = 0.06, 0.21$ and 0.38 for $\sin 2\theta_{13} = 0.1, 0.2$ and 0.3 respectively. For a sufficiently large $\sin 2\theta_{13}$ and a baseline length close to the magic value [14, 15, 16], $P_{e\mu}$ is ideal for probing the octant of θ_{23} .

The probability $P_{\mu\mu}$ is also relevant in neutrino oscillation experiments with neutrino factories. The sensitivity of this probability to θ_{23} is determined by the derivative

$$r \equiv \frac{dP_{\mu\mu}}{d \cos 2\theta_{23}} = -2\alpha \cos 2\theta_{23} + (\alpha + \beta). \quad (15)$$

Since α is negative, the sensitivity r is larger for $\cos 2\theta_{23} > 0$, i.e., $\theta_{23} < \pi/4$. For a measurement performed around a local maximum of $P_{\mu\mu}$, the sensitivity to θ_{23} is completely determined by the coefficient $\alpha + \beta$, since the coefficient α is generally rather suppressed in this case. Along the energy curve denoted by **max1**, $\alpha + \beta$ peaks at 7480 km for $\sin 2\theta_{13} = 0.2$ and it peaks at $L = 7350$ km for $\sin 2\theta_{13} = 0.3$. The values of $\alpha + \beta$ at those peaks are 0.17 and 0.32 respectively. Along the curve **max2**, $\alpha + \beta$ peaks around $L = 10750$ km for both $\sin 2\theta_{13} = 0.2$ and 0.3 with values 0.43 and 0.48 respectively.

For a measurement performed around a local minimum of $P_{\mu\mu}$, the sensitivity to θ_{23} is determined by both coefficients $-\alpha$ and $\alpha + \beta$. Along the energy curve denoted by **min1**, the coefficient $-\alpha$ is always close to unity while the coefficient $\alpha + \beta$ is always suppressed for all baseline lengths. It is understood that the magnitude of $\alpha + \beta$ determines the size of matter effects. Hence the matter effect is small at energies along the curve **min1**. The suppression of $\alpha + \beta$ compared to $-\alpha$ leads to the θ_{23} degeneracy as discussed before. The behavior of $P_{\mu\mu}$ along the energy curve **min2** is more interesting. If the true value of θ_{23} is less than $\pi/4$, the θ_{23} degeneracy from the measurement of $P_{\mu\mu}$ is absent in the baseline range $8300 \leq L/\text{km} \leq 10770$ for $\sin 2\theta_{13} = 0.2$. The above non-degeneracy baseline range extends to $7410 \leq L/\text{km} \leq 10790$ for $\sin 2\theta_{13} = 0.3$. On the other hand, if the true θ_{23} is greater than $\pi/4$, the non-degeneracy baseline range does not exist along the energy curve **min2** for $\sin 2\theta_{13} = 0.2$. For $\sin 2\theta_{13} = 0.3$, the non-degeneracy baseline range is $8270 \leq L/\text{km} \leq 10720$.

The existence of non-degeneracy baseline range along the energy curve **min2** has important implications. It can be seen from Fig. 3 that the curve **min2** lies in between curves **max1** and **max2**. Since the degeneracy of θ_{23} is absent on both **max1** and **max2** for all baselines, it is possible that there exists a non-degeneracy region spanned by ranges of the baseline length and the neutrino energy. For example, with $\sin 2\theta_{13} = 0.2$ and a true value of

TABLE I: The baseline range in which the θ_{23} degeneracy is absent in the probability $P_{\mu\mu}$ for all energy values between the curves **max2** and **max1**. The entry corresponding to $\theta_{23} > \pi/4$ and $\sin 2\theta_{13} = 0.2$ is left blank since, with such set of parameters, there exists no baseline length where the condition for the absence of θ_{23} degeneracy can be satisfied.

θ_{23} octant	$\sin 2\theta_{13} = 0.2$	$\sin 2\theta_{13} = 0.3$
$\theta_{23} < \pi/4$	$8550 \leq L/\text{km} \leq 10680$	$7950 \leq L/\text{km} \leq 10700$
$\theta_{23} > \pi/4$		$8450 \leq L/\text{km} \leq 10680$

θ_{23} less than $\pi/4$, the θ_{23} degeneracy is absent for $8300 \leq L/\text{km} \leq 10770$ for energies along curves **max2**, **min2** and **max1**. It is of great interest to investigate if the θ_{23} degeneracy is also absent for any neutrino energy larger than the value on **max2** and smaller than that on **max1**. By taking all these energies into account, we find that the θ_{23} degeneracy is absent for $8550 \leq L/\text{km} \leq 10680$. For a true value of θ_{23} greater than $\pi/4$ and $\sin 2\theta_{13} = 0.3$, the θ_{23} degeneracy is absent for $8270 \leq L/\text{km} \leq 10720$ for energies along curves **max2**, **min2** and **max1**. However, with all energies between curves **max2** and **max1** considered, we find that the θ_{23} degeneracy is absent for $8450 \leq L/\text{km} \leq 10680$. The non-degeneracy baseline range corresponding to different combinations of θ_{23} and θ_{13} values are summarized in Table I.

It is interesting to compare measurements on $P_{e\mu}$ and $P_{\mu\mu}$ since both oscillations appear in experiments with neutrino factories [29]. The main issue for comparison is on the determination of the true θ_{23} value under the assumption that both the sign of Δm_{31}^2 and the value of $\sin 2\theta_{13}$ are known. Let us begin the discussion with a true value of θ_{23} less than $\pi/4$ and $\sin 2\theta_{13} = 0.2$. For $L < 8550$ km, the appearance mode $\nu_e \rightarrow \nu_\mu$ is useful for probing the octant of θ_{23} , in particular for L close to the magic value, 7600 km. However, the survival mode $\nu_\mu \rightarrow \nu_\mu$ is not as useful since the θ_{23} degeneracy is absent only at energies near **max1** and **max2**. Concerning the sensitivity to θ_{23} , we note that the differentiation of $P_{e\mu}$ with respect to $\cos 2\theta_{23}$ is $-(\alpha + \beta)$. The value of $\alpha + \beta$ increases with L as shown in Fig. 9. It is 0.21 at $L = 7600$ km, and 0.26 at $L = 8550$ km. For $8550 \leq L/\text{km} \leq 10680$, both $\nu_e \rightarrow \nu_\mu$ and $\nu_\mu \rightarrow \nu_\mu$ are useful for probing the octant of θ_{23} . We note that peak positions of $P_{e\mu}$ are mostly around 6 GeV. Hence they overlap with the non-degeneracy energy range of $P_{\mu\mu}$. From Eq. (15) and our assumption of $\theta_{23} < \pi/4$, we find that $P_{\mu\mu}$ is more sensitive to θ_{23}

as compared to $P_{e\mu}$ for the same neutrino energy. For $L > 10680$ km, $\nu_e \rightarrow \nu_\mu$, is again the only useful mode for probing the octant of θ_{23} .

Let us turn to the case where the true value of θ_{23} is greater than $\pi/4$ and $\sin 2\theta_{13} = 0.2$. In such a case, the value for $P_{e\mu}$ is enhanced compared to that with $y > 0$. Furthermore $P_{e\mu}$ is always more sensitive to $\cos 2\theta_{23}$ as compared to $P_{\mu\mu}$ for the same neutrino energy. It is clear that the $\nu_e \rightarrow \nu_\mu$ appearance mode is more useful for probing θ_{23} regardless the baseline length. Although there exists a baseline range where the θ_{23} degeneracy is absent in $P_{\mu\mu}$ for neutrino energies between curves **max2** and **max1**. However this requires a large value of $\sin 2\theta_{13}$, such as $\sin 2\theta_{13} = 0.3$.

It is essential to remark that the above non-degeneracy baseline range is not sensitive to the value of Δm_{31}^2 , which we have so far taken to be $2.4 \cdot 10^{-3}$ eV². Changing the value of Δm_{31}^2 only shifts the probability curves in Fig. 4 and Fig. 6 so that positions for local maxima and local minima of these probabilities shift accordingly. However, the maximal or minimal values of these probabilities remain unchanged. In other words, although the energy curves in Fig. 3 are shifted, the coefficients $-\alpha$ and $\alpha + \beta$ plotted in Fig. 10, which combine to form $P_{e\mu}$ and $P_{\mu\mu}$ (see Eq. (12)), remain the same. The values of these coefficients as functions of the baseline length L then determine the non-degeneracy baseline range.

In conclusion, we have studied the probabilities $P_{e\mu}$ and $P_{\mu\mu}$ for very long baseline neutrino oscillations. We focus on sensitivities of these probabilities to mixing angles θ_{13} , θ_{23} and the CP violation phase δ_{CP} . Taking $\delta_{\text{CP}} = 0$ as an example, we presented contour graphs of $P_{e\mu}$ and $P_{\mu\mu}$ in the $\sin 2\theta_{13} - \cos 2\theta_{23}$ plane for baseline lengths $L = 1000$ km, 5000 km, 10000 km and 12000 km. The energy values chosen for such studies are in the vicinities of either local minima or local maxima of neutrino oscillation probabilities. For each baseline length, we have found that $P_{\mu\mu}$ is more sensitive to $\sin 2\theta_{13}$ at energies around its local maxima while it is more sensitive to $\cos 2\theta_{23}$ at energies around its local minima. On the other hand, the appearance probability $P_{e\mu}$ is sensitive to $\sin 2\theta_{13}$ and $\cos 2\theta_{23}$ only near its local maximum. Such findings have been applied to probe the octant of mixing angle θ_{23} assuming that the angle θ_{13} and the sign of Δm_{31}^2 are known. The appearance probability $P_{e\mu}$ is non-degenerate in θ_{23} . The sensitivity of $P_{e\mu}$ to $\cos 2\theta_{23}$ is studied for baseline lengths from 1000 km to 12000 km. We also studied the sensitivity of $P_{\mu\mu}$ to $\cos 2\theta_{23}$ for the same range of baseline length. We have identified the ranges of neutrino energy and baseline lengths where the θ_{23} degeneracy is absent. We have pointed out that, for a true value of θ_{23}

less than $\pi/4$ and a baseline length between 8000 and 10000 km, the survival mode $\nu_\mu \rightarrow \nu_\mu$ is equally good as the appearance mode $\nu_e \rightarrow \nu_\mu$ for probing the octant of θ_{23} .

Acknowledgements

G.L.L likes to thank D. Indumathi for informative discussions. This work is supported by National Science Council of Taiwan under the grant number NSC 94-2112-M-009-026.

-
- [1] Y. Ashie *et al.* [Super-Kamiokande Collaboration], Phys. Rev. D **71**, 112005 (2005) [arXiv:hep-ex/0501064].
 - [2] Y. Ashie *et al.* [Super-Kamiokande Collaboration], Phys. Rev. Lett. **93** (2004) 101801 [arXiv:hep-ex/0404034].
 - [3] E. Aliu *et al.* [K2K Collaboration], Phys. Rev. Lett. **94** (2005) 081802 [arXiv:hep-ex/0411038].
 - [4] M. H. Ahn *et al.* [K2K Collaboration], Phys. Rev. D **74**, 072003 (2006) [arXiv:hep-ex/0606032].
 - [5] K. Eguchi *et al.* [KamLAND Collaboration], Phys. Rev. Lett. **90** (2003) 021802 [arXiv:hep-ex/0212021].
 - [6] T. Araki *et al.* [KamLAND Collaboration], Phys. Rev. Lett. **94** (2005) 081801 [arXiv:hep-ex/0406035].
 - [7] See G. L. Fogli, E. Lisi, A. Marrone and A. Palazzo, Prog. Part. Nucl. Phys. **57**, 742 (2006) [arXiv:hep-ph/0506083], which contains a list of original references on solar neutrino oscillations.
 - [8] G. L. Fogli and E. Lisi, Phys. Rev. D **54**, 3667 (1996) [arXiv:hep-ph/9604415].
 - [9] M. Apollonio *et al.* [CHOOZ Collaboration], Phys. Lett. B **466**, 415 (1999) [arXiv:hep-ex/9907037].
 - [10] F. Boehm *et al.*, Phys. Rev. D **64**, 112001 (2001) [arXiv:hep-ex/0107009].
 - [11] I. Mocioiu and R. Shrock, Phys. Rev. D **62**, 053017 (2000) [arXiv:hep-ph/0002149]; V. D. Barger, S. Geer, R. Raja and K. Whisnant, Phys. Lett. B **485**, 379 (2000) [arXiv:hep-ph/0004208]; V. D. Barger, S. Geer, R. Raja and K. Whisnant, Phys. Rev. D **62**, 013004 (2000) [arXiv:hep-ph/9911524]; M. Freund, M. Lindner, S. T. Petcov and A. Romanino, Nucl. Phys. B **578**, 27 (2000) [arXiv:hep-ph/9912457]; M. Freund, P. Huber and

- M. Lindner, Nucl. Phys. B **585**, 105 (2000) [arXiv:hep-ph/0004085]; A. Cervera, A. Donini, M. B. Gavela, J. J. Gomez Cadenas, P. Hernandez, O. Mena and S. Rigolin, Nucl. Phys. B **579**, 17 (2000) [Erratum-ibid. B **593**, 731 (2001)] [arXiv:hep-ph/0002108].
- [12] D. Choudhury and A. Datta, JHEP **0507**, 058 (2005) [arXiv:hep-ph/0410266]; D. Indumathi and M. V. N. Murthy, Phys. Rev. D **71**, 013001 (2005) [arXiv:hep-ph/0407336]; S. Choubey and P. Roy, Phys. Rev. D **73**, 013006 (2006) [arXiv:hep-ph/0509197]. D. Indumathi, M. V. N. Murthy, G. Rajasekaran and N. Sinha, Phys. Rev. D **74**, 053004 (2006) [arXiv:hep-ph/0603264].
- [13] We adopt the approach of M. Freund and T. Ohlsson, Mod. Phys. Lett. A **15**, 867 (2000) [arXiv:hep-ph/9909501], by dividing the Earth density regions into the Earth mantle and the Earth core. However we have further introduced the concept of average density to be discussed in details later.
- [14] V. Barger, D. Marfatia and K. Whisnant, Phys. Rev. D **65**, 073023 (2002) [arXiv:hep-ph/0112119].
- [15] P. Huber and W. Winter, Phys. Rev. D **68**, 037301 (2003) [arXiv:hep-ph/0301257].
- [16] A. Y. Smirnov, arXiv:hep-ph/0610198.
- [17] Z. Maki, M. Nakagawa and S. Sakata, Prog. Theor. Phys. **28**, 870 (1962); see also , B. Pontecorvo, Zh. Eksp. Teor. Fiz. **53**, 1717 (1967) [Sov. Phys. JETP **26**, 984 (1968)].
- [18] A. Dziewonski, Earth Structure, Global, in: *The Encyclopedia of Solid Earth Geophysics*, David E. James, ed. (Van Nostrand Reinhold, New York 1989) p. 331.
- [19] M. V. Chizhov and S. T. Petcov, Phys. Rev. D **63**, 073003 (2001) [arXiv:hep-ph/9903424]; M. V. Chizhov and S. T. Petcov, Phys. Rev. Lett. **83**, 1096 (1999) [arXiv:hep-ph/9903399].
- [20] E. K. Akhmedov, Nucl. Phys. B **538**, 25 (1999) [arXiv:hep-ph/9805272].
- [21] S. T. Petcov, Phys. Lett. B **214**, 259 (1988).
- [22] J. Bernabeu, S. Palomares-Ruiz, A. Perez and S. T. Petcov, Phys. Lett. B **531**, 90 (2002) [arXiv:hep-ph/0110071].
- [23] Y. C. Hsu, *Master Thesis*, NCTU (2005).
- [24] See E. K. Akhmedov, R. Johansson, M. Lindner, T. Ohlsson and T. Schwetz, JHEP **0404**, 078 (2004) [arXiv:hep-ph/0402175] and earlier works cited in this paper.
- [25] J. N. Bahcall, M. C. Gonzalez-Garcia and C. Pena-Garay, JHEP **0408** (2004) 016 [arXiv:hep-ph/0406294].

- [26] I. Mocioiu and R. Shrock, JHEP **0111**, 050 (2001) [arXiv:hep-ph/0106139].
- [27] F. Ardellier *et al.* [Double Chooz Collaboration], arXiv:hep-ex/0606025.
- [28] Y. Wang, arXiv:hep-ex/0610024.
- [29] S. Geer, Phys. Rev. D **57**, 6989 (1998) [Erratum-ibid. D **59**, 039903 (1999)]
[arXiv:hep-ph/9712290]; A. De Rujula, M. B. Gavela and P. Hernandez, Nucl. Phys. B **547**,
21 (1999) [arXiv:hep-ph/9811390]; V. D. Barger, S. Geer and K. Whisnant, Phys. Rev. D **61**,
053004 (2000) [arXiv:hep-ph/9906487].
- [30] P. Zucchelli, Phys. Lett. B **532**, 166 (2002).